Chemical Science

Accepted Manuscript

This article can be cited before page numbers have been issued, to do this please use: Y. Shi, K. Tang, J. Zhang, P. Hu, B. Wang, K. Zhao, Y. Zhou, H. Xiang and J. Song, *Chem. Sci.*, 2025, DOI: 10.1039/D5SC01121C.

ROYAL SOCIETY OF CHEMISTRY

rsc.li/chemical-science

View Article Online
DOI: 10.1039/D5SC01121C

ARTICLE

Building Metal-Induced Inherent Chirality: Chiral Stability/Phosphorescence Enhancement via Ring Expansion Strategy of Pt(II) Complexes

Received 00th January 20xx,
Accepted 00th January 20xx

DOI: 10.1039/x0xx00000x

Yingshuang Shi,[a] Ke Tang,[a] Jincheng Zhang,[a] Ping Hu,[a] Bi-Qin Wang,[a] Ke-Qing Zhao,[a] Yuqiao Zhou,[b] Haifeng Xiang,[b]* and Jintong Song[a]*

Chirality is indeed a fundamental aspect of nature, particularly in chemistry and biology. Herein, we have demonstrated a straightforward strategy to create a novel type of metal-induced inherent chirality by expanding coordination rings. Typically, tetracoordinated d^8 Pt(II) complexes with two five-membered coordination rings are 2D square-planar, resulting in the absence of chirality. However, if one of the coordination rings expands into six or seven members, the molecular structures of Pt(II) complexes would transition from a 2D plane to a 3D boat-like configuration. This not only facilitates the construction of inherently chiral scaffolds but also addresses the problem of emission aggregation-caused quenching. Furthermore, the strategy of ring expansion can enhance chiral stability and phosphorescence quantum yield (up to 81.0%). Thus, the present work introduces a new structural motif with promising potential for applications in chiroptical and luminescent materials.

Introduction

Chirality, referring to molecules that cannot fully overlap with their mirror images, is a fundamental property present in nature,[1] and thus the development of novel chiral molecules plays a pivotal role in biochemistry, asymmetric synthesis,[2] supramolecular chemistry,[3] chiral optics,[4] and so on. In general, chirality of organic molecules can be classified into four categories: point, axial, helical, and planar.[5] The term "inherently chiral" was first suggested by Böhmer for chiral calixarenes which do not strictly fall into definitions of other types of chirality.[6] Later, a more general definition was formulated in 2004 by the group of Mandolini and Schiaffino.[7] It states that inherent chirality derives from the "introduction of a curvature in an ideal planar structure that is devoid of symmetry axes in its bidimensional representation".[8] Since then, the concept of inherent chirality has been increasingly used to denote chirality arising from the rigid structures in both medium-sized rings (no less than seven-membered ring)[9] and large-sized rings (such as rotaxanes, catenanes, fullerenes, cavitands, and capsular assemblies).[10] However, these pure organic molecules usually exhibit fluorescence.[9a,11]

Cyclometalated Pt(II) complexes have been extensively investigated in the past two decades owing to their rich phosphorescence properties and wide applications in phosphorescent organic light emitting diodes,[12] chemosensors,[13] bio-imaging,[14] circularly polarized luminescence (CPL),[5a,5d,15] and so on. Typically, tetracoordinated d^8 Pt(II) complexes with two five-membered coordination rings are 2D square-planar,[16] resulting in the lack of chirality. Moreover, these square-planar molecules are far more likely to encounter the problem of emission "aggregation-caused quenching" (ACQ), because they readily form dimers through not only intermolecular π–π stacking interactions, but also Pt^{II}–Pt^{II} interactions.[14] Therefore, the chirality of Pt(II) complexes is primarily introduced by chiral ligands.[5d,15,17] Although there are limited examples of chiral Pt(II) complexes with achiral ligands,[18] their chiroptical properties, especially CPL, have seldom been reported before, mainly due to not only the weak chirality but also low phosphorescence quantum yields (Φ). Herein, we have demonstrated a straightforward strategy to build a novel type of metal-induced inherent chirality by expanding coordination rings (Fig. 1). When using N_1^O, N_2^O, N^P, N^PS, and N^PO bidentate ligands, one of coordination rings expands into six or seven members. The molecular structures of Pt(II) complexes would change from 2D plane into 3D boat-like configuration, which not only facilitates the construction of inherently chiral scaffolds but also resolves the ACQ problem. Moreover, the strategy of ring expansion can improve chiral stability and phosphorescence quantum yield (up to 81.0%). Furthermore, the resultant enantiomers of complexes can be separated by chiral high-performance liquid chromatography (HPLC) and their absolute configuration is confirmed by X-ray diffraction, circular dichroism, CPL, and density functional theory calculation.

[a] College of Chemistry and Materials Science, Sichuan Normal University, Chengdu 610066, China. E-mail: jintongsong@sicnu.edu.cn
[b] College of Chemistry, Sichuan University, Chengdu 610065, China. E-mail: xianghaifeng@scu.edu.cn
Electronic Supplementary Information (ESI) available. See DOI: 10.1039/x0xx00000x

View Article Online
DOI: 10.1039/D5SC01121C

ARTICLE

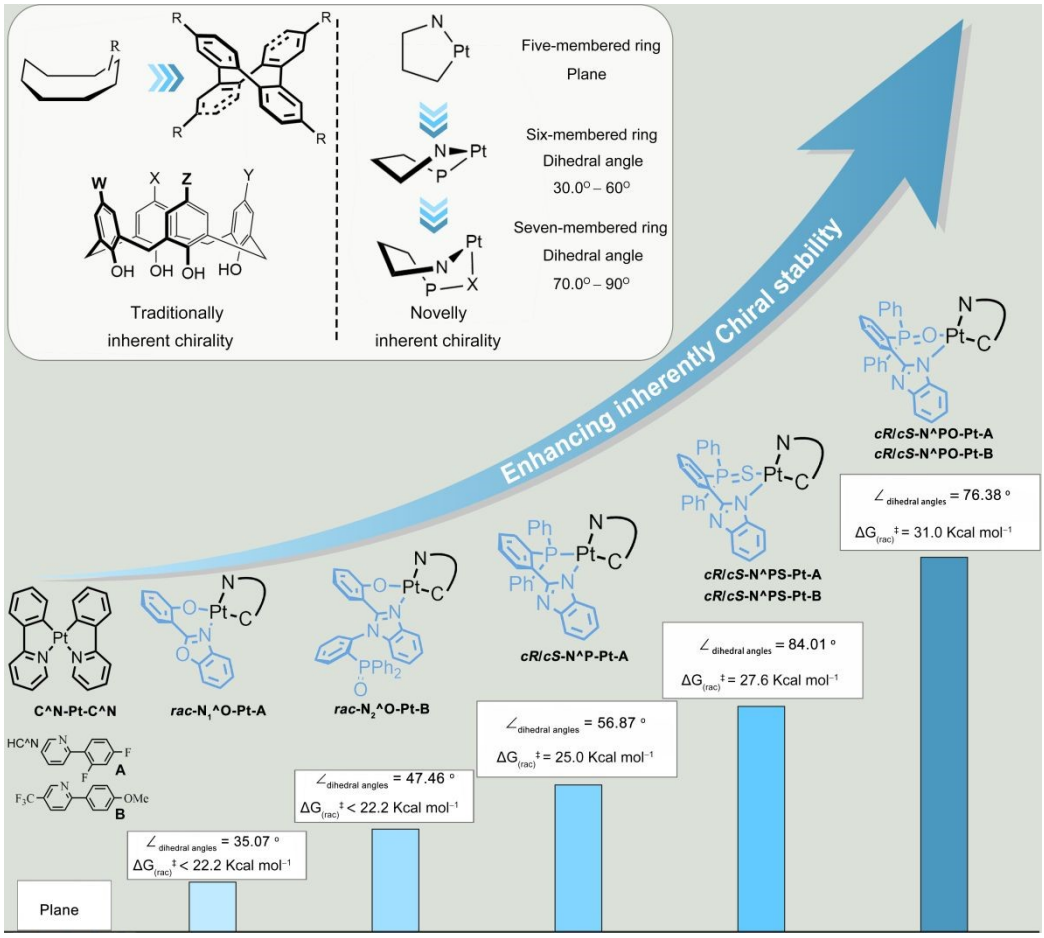

Fig. 1. The designed scheme and chemical structures of inherently chiral Pt(II) complexes (∠dihedral angles : angle between the phenyl plane and the PtC^N coordination plane; $\Delta G_{(rac)}^{\ddagger}$: racemization energy barriers of inherently chiral Pt(II) complexes).

Results and Discussion

Synthesis and Characterizations. The synthetic methods for the ligands and Pt(II) complexes are detailed in the Supporting Information. Initially, we utilized **N_1^O**, **N_2^O**, and **N^P** ligands to synthesize the Pt(II) complexes with six-membered coordination rings. **N^PS** and **N^PO** ligands were used to prepare the Pt(II) complexes with seven-membered coordination rings. Single crystals of ***rac*-N_1^O-Pt-A** (CCDC: 2378928), ***rac*-N_2^O-Pt-B** (CCDC: 2378929), ***rac*-N^P-Pt-A** (CCDC: 2378930), ***rac*-N^PS-Pt-A** (CCDC: 2378935), ***rac*-N^PO-Pt-A** (CCDC: 2378936), ***rac*-N^PS-Pt-B** (CCDC: 2378939), and ***rac*-N^PO-Pt-B** (CCDC: 2386027) were obtained through slow diffusion and evaporation of a hexane/CH_2Cl_2 solution.

Firstly chiral HPLC was used to analyze and separate enantiomers of the Pt(II) complexes. For ***rac*-N_1^O-Pt-A** and ***rac*-N_2^O-Pt-B** (Fig. S1), there exists only one chromatographic peak in the HPLC trace. The possible reason is that the steric hindrance of **N_1^O** and **N_2^O** is too small to stabilize chirality in solution. With strong steric hindrance from two phenyl groups in triphenyl phosphine, ***rac*-N^P-Pt-A**, ***rac*-N^PS-Pt-A**, ***rac*-N^PO-Pt-A**, ***rac*-N^PS-Pt-B**, and ***rac*-N^PO-Pt-B** have two separated chromatographic peaks featuring a 1:1 ratio of the area (Fig. 2). The first peak (black line) refers to the optical pure ***cR*-N^P-Pt-A**, ***cR*-N^PS-Pt-A**, ***cR*-N^PO-Pt-A**, ***cR*-N^PS-Pt-B**, and ***cR*-N^PO-Pt-B**, while the second one (red line) corresponds to the ***cS*-N^P-Pt-A**, ***cS*-N^PS-Pt-A**, ***cS*-N^PO-Pt-A**, ***cS*-N^PS-Pt-B**, and ***cS*-N^PO-Pt-B** (see the later discussion). Enantiopure ***cR*** and ***cS*-Pt(II)** complexes (>98% ee) were collected by chiral HPLC, albeit in recovered yield inferior to 30%, respectively.

View Article Online
DOI: 10.1039/D5SC01121C

ARTICLE

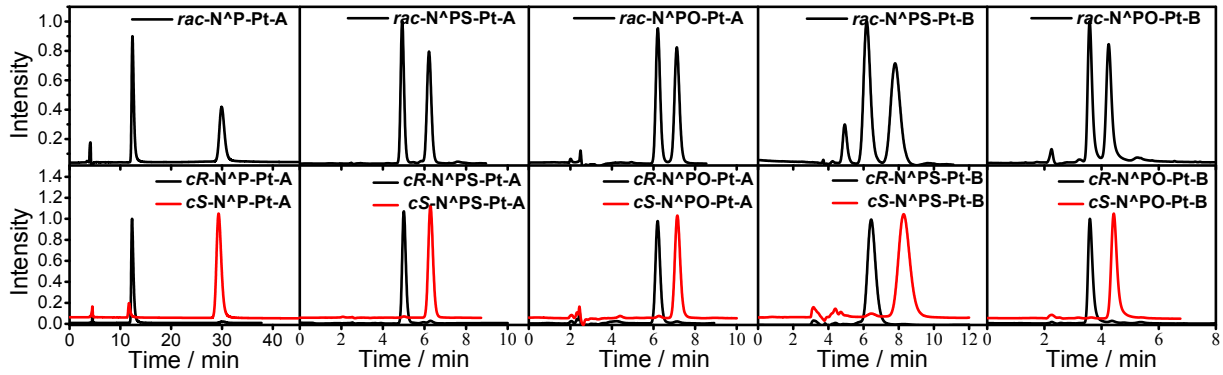

Fig. 2. Top: chiral HPLC traces of ***rac*-N^P-Pt-A**, ***rac*-N^PS-Pt-A**, ***rac*-N^PO-Pt-A**, ***rac*-N^PS-Pt-B**, and ***rac*-N^PO-Pt-B**. Bottom: chiral HPLC traces of enantiopure (*cR*) (black line) and (*cS*) (red line) Pt(II) complexes.

Table 1. Room-temperature photophysical properties of binuclear Pt(II) complexes.

Compounds	medium	λ_{abs}/nm (ε/dm3 mol^{-1} cm^{-3})	λ_{em}/nm	Φ_{PL}	τ_P/μs
***rac*-N^P-Pt-A**	CH_2Cl_2	316 (1.84×10^4), 380 (2.99×10^3)	/	/	/
	Powder	/	468/496/535	0.45%	1.11
***rac*-N^PS-Pt-A**	CH_2Cl_2	267 (1.68×10^4), 318 (9.01×10^3), 358 (4.25×10^3)	/	/	/
	Powder	/	466/500/535	6.61%	0.97
***rac*-N^PO-Pt-A**	CH_2Cl_2	247 (2.47×10^4), 317 (1.02×10^4), 375 (1.60×10^3)	/	/	/
	Powder	/	473/502/544	29.4%	0.94
***rac*-N^PS-Pt-B**	CH_2Cl_2	296 (1.22×10^4), 410 (1.43×10^3)	/	/	/
	Powder	/	506/538	3.39%	8.51
***rac*-N^PO-Pt-B**	CH_2Cl_2	311 (1.48×10^4), 419 (1.89×10^3)	/	/	/
	Powder	/	521/549	81.0%	9.27

Photophysical Properties and Calculations.

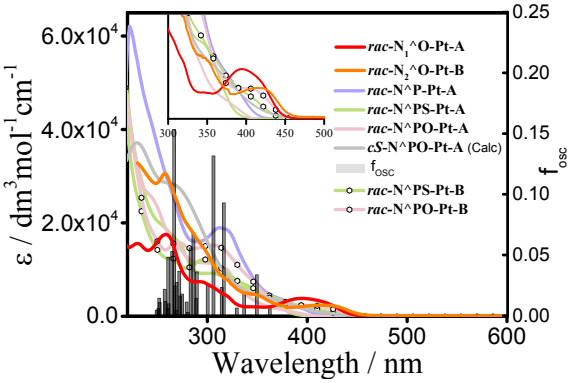

Fig 3. Experimental absorption spectra of Pt(II) complexes in CH_2Cl_2 solution (5.0 x 10^{-5} mol dm^{-3}).

Table 1 presents the UV/visible absorption and emission data of Pt(II) complexes at room temperature. As illustrated in Fig 3, ***rac*-N$_1$^O-Pt-A**, ***rac*-N^P-Pt-A**, ***rac*-N^PO-Pt-A**, and ***rac*-N^PS-Pt-A** with a common HC^N ligand of 2-(4′,6′-difluorophenyl)pyridine (**A**) exhibit a low-energy absorption band at λ_{abs} = 402, 380, 375, and 358 nm, respectively, demonstrating a gradual blue shift. This trend contrasts with the trend of corresponding dihedral angles, which is 35.07°, 56.87°, 76.38°, and 84.01° for ***rac*-N$_1$^O-Pt-A**, ***rac*-N^P-Pt-A**, ***rac*-N^PO-Pt-A**, and ***rac*-N^PS-Pt-A** respectively. A bigger dihedral angle would lead to a smaller degree of conjugation and a bule-shifted absorption band consequently (see the later discussion). ***rac*-N^PO-Pt-A**, and ***rac*-N^PO-Pt-B** with the same **N^PO** but different C^N ligands display a low-energy absorption band at λ_{abs} = 375, and 419 nm, respectively. All above results indicate that not only **N$_1$^O**, **N$_2$^O**, **N^P**, **N^PS**, and **N^PO** but also HC^N ligands have obvious impact on absorption spectra.

Density functional theory (DFT) and time-dependent DFT (TD-DFT) calculations were conducted using the Gaussian 09 program package to investigate the mechanisms of excited states and transitions. In dilute CH_2Cl_2 solution, both the absorption spectral bands and molar absorption coefficients (ε) of Pt(II) complexes are well-replicated by theoretical computations (Fig. 3, S2–S4). The low-energy absorption

View Article Online DOI: 10.1039/D5SC01121C

band of ***rac*-N^PS-Pt-A**, ***rac*-N^PO-Pt-A**, and ***rac*-N^P-Pt-A** is 358 nm, 375 nm, and 380 nm, respectively, which is accurately reproduced by TD-DFT calculations (calculated λ_{abs} = 362 nm, 365 nm, and 388 nm for ***cS*-N^PS-Pt-A**, ***cS*-N^PO-Pt-A**, and ***cS*-N^P-Pt-A**, respectively. These low-energy absorption bands are primarily attributed to the transition from the highest occupied molecular orbital (HOMO) to the lowest unoccupied molecular orbital (LUMO) with contributions exceeding 80%, and the corresponding oscillator strength (f_{osc}) is 0.0075, 0.0288, and 0.0389 for ***cS*-N^PS-Pt-A**, ***cS*-N^PO-Pt-A**, and ***cS*-N^P-Pt-A**, respectively. The energy level diagram and frontier molecular orbitals indicate that the electron cloud of the HOMO is predominantly contributed by the electron-rich Pt(II) ions and the 1H-benzo[d]imidazole segments of the **N^P**, **N^PS**, and **N^PO** ligands, while the LUMO's electron cloud is mainly derived from the electron-deficient HC^N ligands (Fig. 4). Consequently, the low-energy absorption bands are primarily attributed to metal-to-ligand charge transfer (MLCT) from Pt(II) ions to C^N ligands, as well as ligand-to-ligand charge transfer (LLCT) from 1H-benzo[d]imidazole to HC^N ligands. Not only **N^P**, **N^PS**, and **N^PO** ligands but also HC^N ligands have obvious contributions on low-energy absorption bands, which is in accord with UV/visible absorption data (Table 1).

All the Pt(II) complexes are weakly emissive or non-emissive in dilute degassed CH_2Cl_2 solution. In comparison with solution samples, but their powders show significant aggregation-induced emission (AIE)[19] with the promising quantum yields (3.76%, 4.40%, 0.45%, 6.61%, 29.4%, 3.39%, and 81.0% for ***rac*-N_1^O-Pt-A**, ***rac*-N_2^O-Pt-B**, ***rac*-N^P-Pt-A**, ***rac*-N^PS-Pt-A**, ***rac*-N^PO-Pt-A**, ***rac*-N^PS-Pt-B**, and ***rac*-N^PO-Pt-B**, respectively) (Fig. 5 and S5, and Table 1 and S1). Based on their relatively long emission decay lifetimes in the microsecond range (μs, Fig. S6, S7, and Table 1) and significant Stokes shifts (ranging from 140 nm to 170 nm) between the absorption and emission bands, the emission from Pt(II) complexes can be classified as phosphorescence, originating from triplet excited states. As illustrated in Fig S8, the frontier molecular orbitals in the triplet excited states of Pt(II) complexes (in CH_2Cl_2 solution) are analogous to those in singlet excited states, suggesting that their phosphorescence predominantly arises from ^{3}MLCT and ^{3}LLCT.

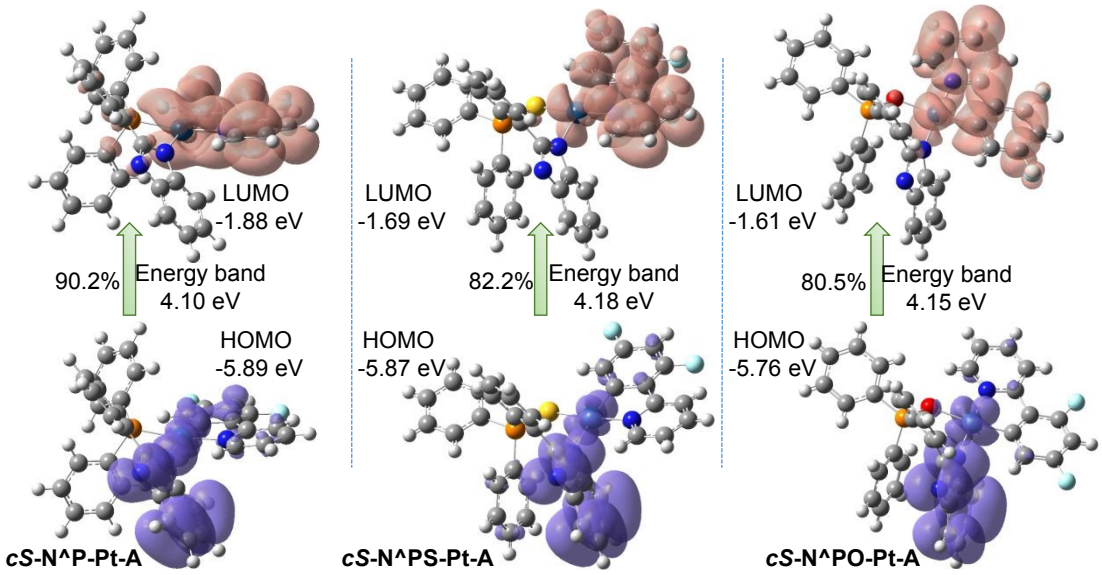

Fig 4. Energy level diagram and frontier molecular orbitals of ***cS*-N^P-Pt-A**, ***cS*-N^PS-Pt-A**, and ***cS*-N^PO-Pt-A** (in CH_2Cl_2).

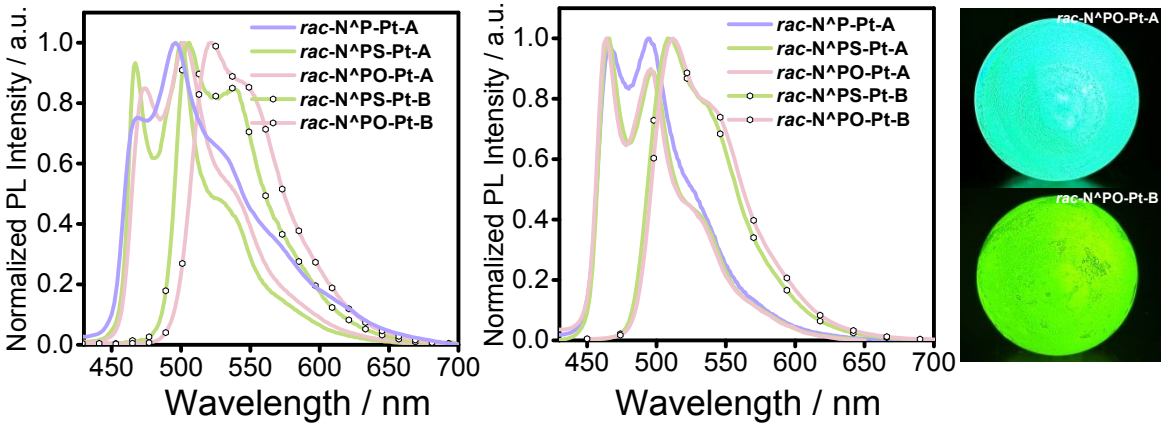

Fig 5. PL spectra of ***rac*-N^P-Pt-A**, ***rac*-N^PS-Pt-A**, ***rac*-N^PO-Pt-A**, ***rac*-N^PS-Pt-B**, and ***rac*-N^PO-Pt-B** in powder and doped film. Photographs of ***rac*-N^PO-Pt-A**, and ***rac*-N^PO-Pt-B** in powder under 365 nm UV lamp.

View Article Online
DOI: 10.1039/D5SC01121C

ARTICLE

X-ray Single-Crystal Structures. The molecular structure and packing in X-ray single crystal of ***rac*-N^PS-Pt-A** and ***rac*-N^PO-Pt-A** are illustrated in Fig 6. Unlike those of the traditional inherently chiral molecules, according to the definition of calixarenes, curvature is denoted by 'c', with clockwise being '*cR*' and counterclockwise being '*cS*'.[12,13] The core skeletons of these Pt(II) complexes are chiral (Fig. 1), such metal-induced chirality can be also defined as inherent chirality for simplicity. An ideal observer standing on the cabin (the concave side of the surface) will see a seven-membered ring (Pt, O, P, C, C, C, and N atom) at the side of boat. The clockwise or a counterclockwise array of the three highest priority atoms designates as (*cR*) or (*cS*), respectively, as shown in Fig 6. As anticipated, there are a pair of (*cR*)/(*cS*) enantiomers in their single crystals [***cR*-N^PO-Pt-A** and ***cS*-N^PO-Pt-A**; ***cR*-N^PS-Pt-A** and ***cS*-N^PS-Pt-A**], corroborating the viability of our design strategy. Additionally, the enantiomers of ***rac*-N_1^O-Pt-A**, ***rac*-N_2^O-Pt-B**, ***rac*-N^PS-Pt-B**, and ***rac*-N^PO-Pt-B** (Fig. S9–S11) are also discernible within the single-crystal structures.

The photoluminescence properties of Pt(II) complexes are significantly influenced by their molecular structures and arrangements. There are not freely rotating groups for ***rac*-N_1^O-Pt-A**, and ***rac*-N_2^O-Pt-B**, however, their solutions are weakly emissive. This suggests that the molecular backbone vibration to promote the non-radiative decay process.[11,20] The other Pt(II) complexes contain not only molecular backbone vibration but also C–P-bond-linked phenyl groups, which are capable of free motion and consequently offer possible pathway for the non-radiative annihilation of their excited states in solution. On the other hand, there are many strong intermolecular interactions, such as many F–H (2.627–2.933 Å), C–H (2.665–2.886 Å), N–H (2.551–2.862 Å), O–H (2.410–2.713 Å), and H–H (2.350–2.769 Å) interactions (Fig. S9–S12) in the single crystals of ***rac*-N^P-Pt-A**, ***rac*-N^PS-Pt-A**, ***rac*-N^PO-Pt-A**, ***rac*-N^PS-Pt-B**, **and *rac*-N^PO-Pt-B**. These strong intermolecular interactions can inhibit the rotation of C–P single bonds. The metal–metal interactions can significantly alter the photophysical properties of the complexes, such as red-shifted spectra and changes in the nature of the charge transfer transitions.[21] Moreover, these resultant Pt(II) complexes adopt a 3D boat-like structures, which hinders intermolecular face-to-face π–π stacking interaction and Pt^{II}–Pt^{II} interactions (5.871–8.033 Å, Fig. S10–12) between adjacent complexes intermolecular. Under the above synergistic effects, these Pt(II) complexes exhibit substantial AIE phenomenon[19] (0.45%, 6.61%, 29.4%, 3.39%, and 81.0% for ***rac*-N^P-Pt-A**, ***rac*-N^PS-Pt-A**, ***rac*-N^PO-Pt-A**, ***rac*-N^PS-Pt-B**, and ***rac*-N^PO-Pt-B**, respectively).

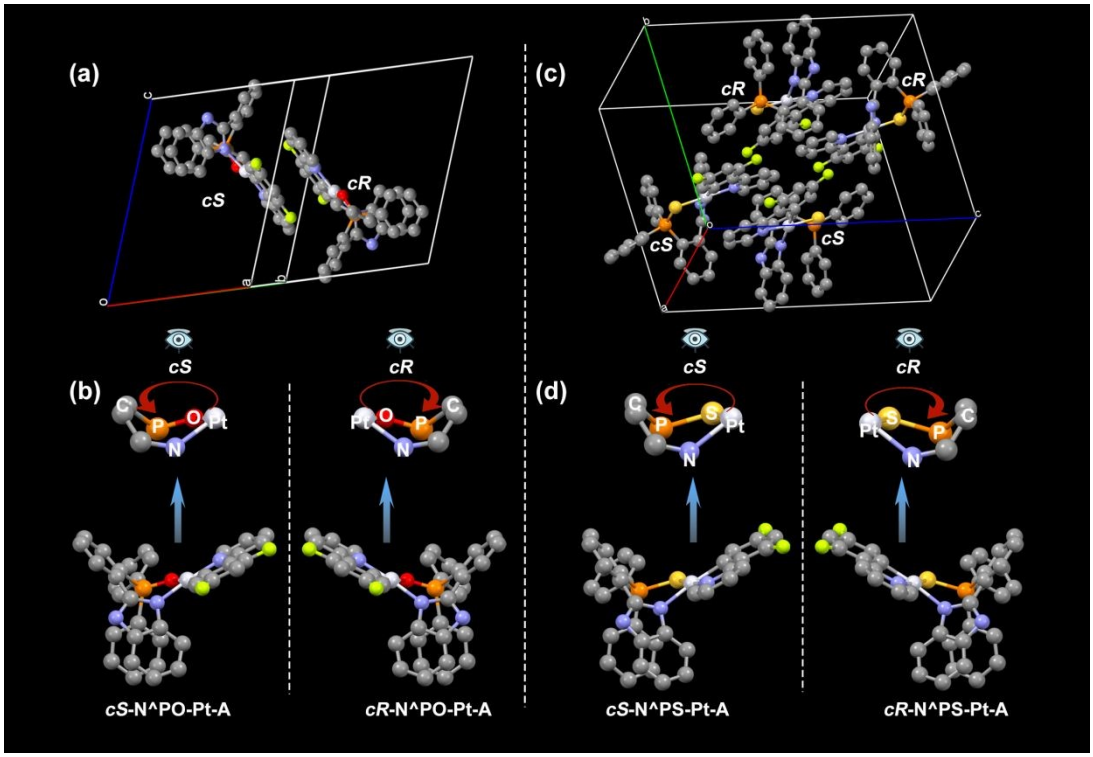

Fig 6. X-ray single-crystal structures of ***rac*-N^PO-Pt-A**: (a) one crystal cell; (b) ***cR*-N^PO-Pt-A** and ***cS*-N^PO-Pt-A** molecular structures and the definition of (c*R*)/(c*S*) chirality (some atoms are omitted); X-ray single-crystal structures of ***rac*- N^PS-Pt-A**: (c) one crystal cell; (d) ***cR*-N^PS-Pt-A** and ***cS*-N^PS-Pt-A** molecular structures and the definition of (c*R*)/(c*S*) chirality (some atoms are omitted).

View Article Online
DOI: 10.1039/D5SC01121C

ARTICLE

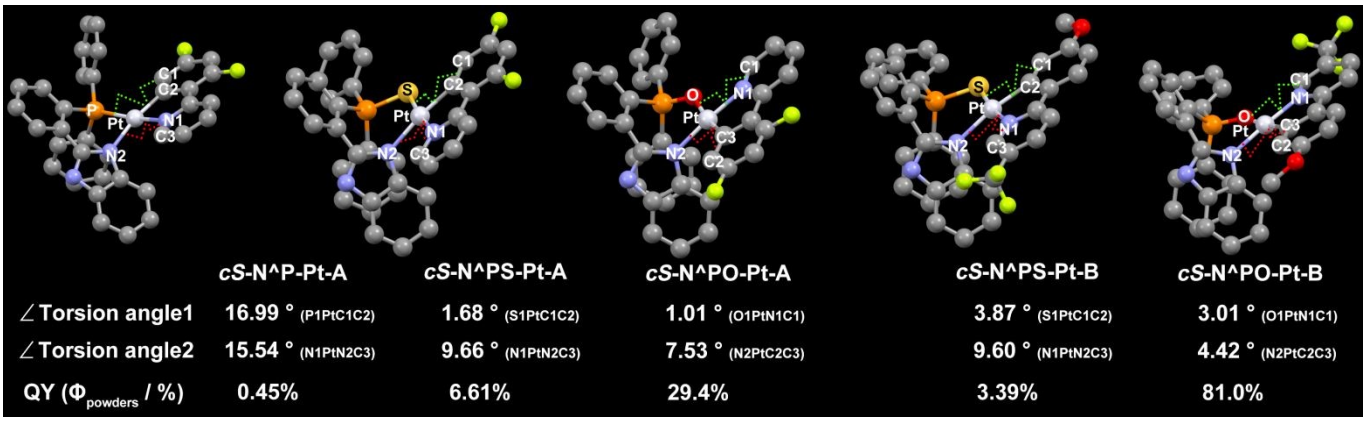

Fig 7. The relationship between emission quantum yields and the torsion angels of coordinated atoms of among these representative products ***cS*-N^P-Pt-A**, ***cS*-N^PS-Pt-A**, ***cS*-N^PO-Pt-A**, ***cS*-N^PS-Pt-B**, and ***cS*-N^PO-Pt-B**.

In theory, the emission quantum yield of a square-planar Pt(II) complex is strongly dependent on the planeness of coordination. The less torsion, the higher quantum yield. For all the AIE-active Pt(II) complexes, the Pt atoms and HC^N ligands are nearly coplanar. However, their emission quantum yields are quite different. The torsion angle of the C1–C2–Pt–P, C1–C2–Pt–S, C1–N1–Pt–O, C1–C2–Pt–S, C1–N1–Pt–O is 16.99°, 1.68°, 1.01°, 3.87°, and 3.01° for ***cS*-N^P-Pt-A**, ***cS*-N^PS-Pt-A**, ***cS*-N^PO-Pt-A**, **(*cS*)N^PS-Pt-B**, and ***cS*-N^PO-Pt-B**, respectively. Additionally, the torsion angle of C3–N1–Pt–N2, C3–N1–Pt–N2, C2–C3–Pt–N2, C3–N1–Pt–N2, C2–C3–Pt–N2 is 15.54°, 9.66°, 7.53°, 9.60°, and 4.42° for **(*cS*)N^P-Pt-A**, ***cS*-N^PS-Pt-A**, ***cS*-N^PO-Pt-A**, ***cS*-N^PS-Pt-B**, and ***cS*-N^PO-Pt-B**, respectively. ***cS*-N^PO-Pt-A**, and ***cS*-N^PO-Pt-B** have less distorted square-planar geometry, resulting in their high emission quantum yields (Fig. 7).

Racemization experiment. The chirality of these Pt(II) complexes is originated from their 3D boat-type structures. If the cocked phenyl group in N_1^O, N_2^O, N^P, N^PS, and N^PO ligands flips down into the coplane with the coordination system, the racemization would occur. Therefore, the chiral stability is determined by the dihedral angle between the phenyl group and coordination system. The dihedral angles of these Pt(II) complexes exhibit a positive correlation with both the size of the ring and the peripheral substituent groups. It is reported that enantiomers with racemization energy barriers more than 22.2 kcal/mol could be separable at room temperature.[22] The chirality of ***rac*-N_1^O-Pt-A** and ***rac*-N_2^O-Pt-B** is not stable in soultion, because they don't have large steric group of triphenyl phosphine. The chirality of other Pt(II) complexes with triphenyl phosphine group is stable and separable. The dihedral angle of ***cS*-N_1^O-Pt-A**, ***cS*-N_2^O-Pt-B**, ***cS*-N^P-Pt-A**, ***cS*-N^PO-Pt-A**, and ***cS*-N^PS-Pt-A** is measured to be 35.07°, 47.46°, 56.87°, 76.38°, and 84.01°, respectively (Fig. 8a). Following Curran's methodology,[23] the fitting of *cS*-N^P-Pt-A, *cS*-N^PO-Pt-A, and *cS*-N^PS-Pt-A are to calculate the flipping energy barrier. The energy barrier calculated by fitting has been shown in Figure 8b, which are 25.0 kcal·mol^{-1} (half life $t_{1/2}$ = 1.50 days at 25 °C), 27.6 kcal·mol^{-1} ($t_{1/2}$ = 0.31 years at 25 °C), and 31.0 kcal·mol^{-1} ($t_{1/2}$ = 94 years at 25 °C), respectively (Table S1–S3). The sulfur atom in the N^PS ligands is undoubtedly larger than the oxygen atom in the N^PO ligands. Therefore, the increased repulsive force from the sulfur atom results in a more distorted seven-membered ring in ***cS*-N^PS-Pt-A** compared to ***cS*-N^PO-Pt-A**, which is evidenced by the larger dihedral angle of ***cS*-N^PS-Pt-A** (84.01°) than that of ***cS*-N^PO-Pt-A** (76.38°).

View Article Online
DOI: 10.1039/D5SC01121C

ARTICLE

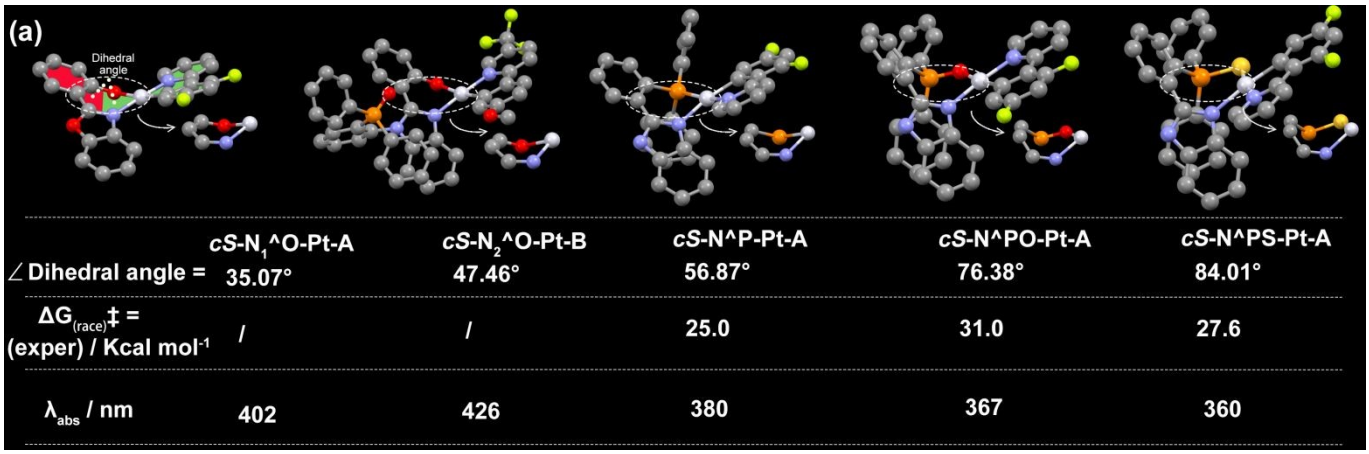

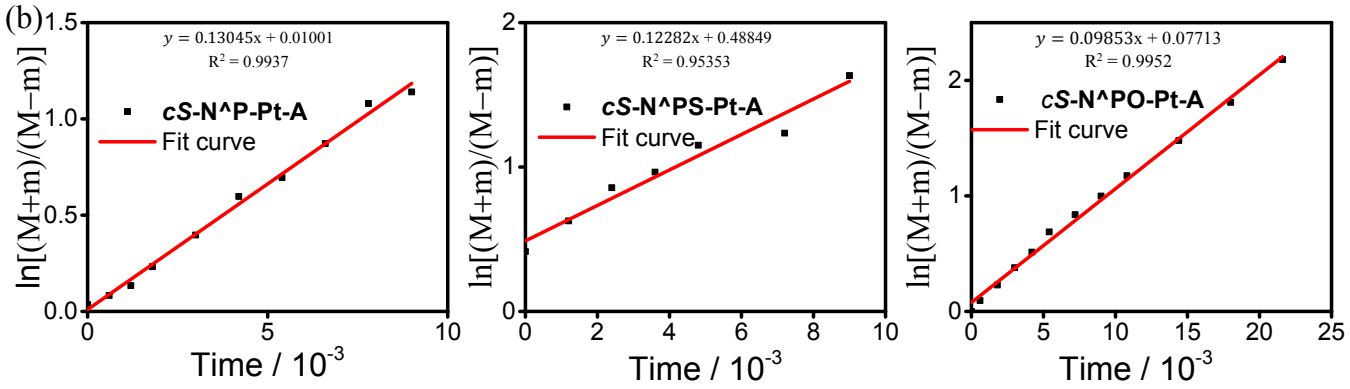

Fig 8. (a) X-ray single-crystal structures, dihedral angles, experimental interconversion energy barriers of ***cS*-N$_1$^O-Pt-A**, ***cS*-N$_2$^O-Pt-B**, ***cS*-N^P-Pt-A**, ***cS*-N^PO-Pt-A**, **and *cS*-N^PS-Pt-A**; (b) Investigations of rotation barriers of ***cS*-N^P-Pt-A**, ***cS*-N^PO-Pt-A**, and **(*cS*)N^PS-Pt-A**.

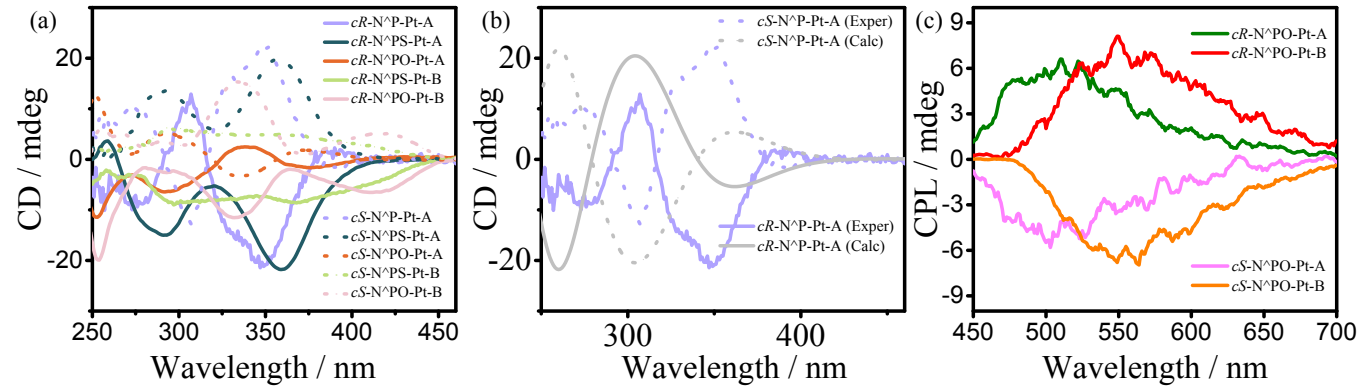

Fig 9. (a) CD spectra of Pt(II) complexes in dilute CH_2Cl_2 solution (3.0×10^{-5} mol dm^{-3}); (b) Experimental and calculated CD spectra of ***cR*/*cS*-N^P-Pt-A** complexes in dilute CH_2Cl_2 solution; (c) CPL spectra of Pt(II) complexes in powder.

Chiroptical Properties. The chiroptical properties of Pt(II) complexes were examined using circular dichroism (CD) and CPL spectroscopy (Fig. 9). The CD spectra of the enantiomers in dilute CH_2Cl_2 solution (3.0×10^{-5} mol dm^{-3}) exhibit perfect mirror images. The calculated CD spectra closely correspond to the experimental spectra, further confirming the absolute stereochemistry. Analyzing the calculations,

the CD peaks in the range of 350–450 nm can be attributed to the MLCT and LLCT. The chirality of square-planar d^8 Pt(II) complexes is predominantly introduced through the use of chiral ligands, and there are only limited examples of chiral Pt(II) complexes derived from achiral ligands. However, the $|g_{lum}|$ of these chiral Pt(II) complexes typically range around 10^{-3}, and they often exhibit low photoluminescence quantum yields (Φ). The CPL spectra of the resulting Pt(II) complexes in the solid state are shown in Figure 9, and closely correspond to their photoluminescence (PL) spectra. The $|g_{PL}|$ values at the emission maxima (λem) are approximately 1.0–2.0 × 10^{-3}, which are comparable to those observed in typical small organic molecules.[24] Nevertheless, both the luminescence dissymmetry factors and quantum yields require further enhancement to meet practical application standards. Recent studies have shown that chiral Pt(II) complexes can achieve markedly enhanced g_{lum} values via the construction of chiral supramolecular architectures through intermolecular interactions,[12g,25] highlighting a compelling strategy for advancing next-generation CPL-active materials.

Conclusions

In this study, we developed a straightforward and efficient strategy to construct a novel type of (*cR*)/(*cS*) inherent chirality through metal coordination. These Pt(II) complexes, featuring a boat-type conformation, face challenges related to the absence of metal-induced chirality and the risk of ACQ for square-planar complexes. They exhibit intense blue-green and green phosphorescence with high quantum yields and moderate asymmetry factors. These findings provide valuable insights into the design of metal-doped chiral materials and their potential applications.

Data availability

The data supporting this article have been included as part of the ESI.† Deposition number 2378928, 2378929, 2378930, 2378935, 2378936, 2378939, and 2386027 contains the supplementary crystallographic data for this paper. The data can be obtained free of charge via the joint Cambridge Crystallographic Data Centre (CCDC).

Author Contributions

Y. S. Shi, K. Tang, and J. C. Zhang conducted all of the reactions and data collection. J. T. Song conducted DFT calculations, experimental mechanistic studies some aspects of characterization of the compounds, and wrote the manuscript. Y. Q. Zhou contributed to the crystal testing. P. Hu, B-Q Wang, and K-Q Zhao contributed to supervision and direction of the project. H. F. Xiang conceptualized and directed the project and revise the manuscript. All the authors contributed to scientific discussions.

Conflicts of interest

There are no conflicts to declare.

Acknowledgements

The authors gratefully acknowledge financial support from the National Natural Science Foundation of China (Nos.22405184 and 21871192) and the Natural Science Foundation of Sichuan Province, China (no. 2025ZNSFSC0118). We would like to thank Prof. Dr. Peng Wu & Dr. Yanying Wang of Analytical & Testing Center, Sichuan University for their assistance on transient fluorescence. We also would like to thank Prof. Dr. Zong-Xiang Xu of Department of Chemistry, Southern University of Science and Technology for X-ray diffraction work and single-crystal analysis.

Notes and references

1. K. P. Meurer and F. Vogtle, *Top. Curr. Chem.*, 1985, **127**, 1-76.
2. (a) P. Kočovský, Š. Vyskočil and M. Smrčina, *Chem. Rev.*, 2003, **103**, 3213-3246; (b) D. Zhang, A. Martinez and J.-P. Dutasta, *Chem. Rev.*, 2017, **117**, 4900-4942.
3. (a) M. Liu, L. Zhang and T. Wang, *Chem. Rev.*, 2015, **115**, 7304-7397; (b) L.-J. Chen, H.-B. Yang and M. Shionoya, *Chem. Soc. Rev.*, 2017, **46**, 2555-2576.
4. L. Zhang, H.-X. Wang, S. Li and M. Liu, *Chem. Soc. Rev.*, 2020, **49**, 9095-9120.
5. (a) Z.-L. Gong, T.-X. Dan, J.-C. Chen, Z.-Q. Li, J. Yao and Y.-W. Zhong, *Angew. Chem. Int. Ed.*, 2024, **63**, e202402882; *Angew. Chem*. 2024, **136**, e202402882; (b) N. Hellou, M. Srebro-Hooper, L. Favereau, F. Zinna, E. Caytan, L. Toupet, V. Dorcet, M. Jean, N. Vanthuyne, J. A. G. Williams, L. Di Bari, J. Autschbach and J. Crassous, *Angew. Chem. Int. Ed.*, 2017, **56**, 8236-8239; *Angew. Chem.* 2017, **129**, 8348-8351 (c) G. Mazzeo, S. Ghidinelli, R. Ruzziconi, M. Grandi, S. Abbate and G. Longhi, *ChemPhotoChem*, 2022, **6**, e202100222; (d) M. Ikeshita, N. Hara, Y. Imai and T. Naota, *Inorg. Chem.*, 2023, **62**, 13964-13976.
6. V. Böhmer, D. Kraft and M. Tabatabai, *J. Inclusion Phenom. Mol. Recognit. Chem.*, 1994, **19**, 17-39.
7. A. Dalla Cort, L. Mandolini, C. Pasquini and L. Schiaffino, *New J. Chem.*, 2004, **28**, 1198-1199.
8. A. Szumna, *Chem. Soc. Rev.*, 2010, **39**, 4274-4285.
9. (a) Y. Liu, Z. Ma, Z. Wang and W. Jiang, *J. Am. Chem. Soc.*, 2022, **144**, 11397-11404; (b) J.-H. Li, X.-K. Li, J. Feng, W. Yao, H. Zhang, C.-J. Lu and R.-R. Liu, *Angew. Chem. Int. Ed.*, 2024, **63**, e202319289; *Angew. Chem*. 2024, **136**, e202319289.
10. (a) S. Tong, J.-T. Li, D.-D. Liang, Y.-E. Zhang, Q.-Y. Feng, X. Zhang, J. Zhu and M.-X. Wang, *J. Am. Chem. Soc.*, 2020, **142**, 14432-14436; (b) W. H. Powell, F. Cozzi, G. P. Moss, C. Thilgen, R. J.-R. Hwu and A. Yerin, *Pure Appl. Chem.*, 2002, **74**, 629-695; (c) E. M. G. Jamieson, F. Modicom and S. M. Goldup, *Chem. Soc. Rev.*, 2018, **47**, 5266-5311; (d) C. A. Schalley, W. Reckien, S. Peyerimhoff, B. Baytekin and F. Vögtle, *Chem. Eur. J.*, 2004, **10**, 4777-4789.
11. (a) Z. Zhao, X. Zheng, L. Du, Y. Xiong, W. He, X. Gao, C. Li, Y. Liu, B. Xu, J. Zhang, F. Song, Y. Yu, X. Zhao, Y. Cai, X. He, R. T. K. Kwok, J. W. Y. Lam, X. Huang, D. Lee Phillips, H. Wang and B. Z. Tang, *Nat. Commun.*, 2019, **10**, 2952; (b) J.-W. Han, X.-S. Peng and H. N. C. Wong, *Natl. Sci. Rev.*, 2017, **4**, 892-916.
12. (a) M. A. Baldo, D. F. O'Brien, Y. You, A. Shoustikov, S. Sibley, M. E. Thompson and S. R. Forrest, *Nature*, 1998, **395**, 151-154; (b) E. V. Puttock, M. T. Walden and J. A. G. Williams, *Coord. Chem. Rev.*, 2018, **367**, 127-162; (c) C.-W. Chan, L.-K. Cheng and C.-M. Che, *Coord. Chem. Rev.*, 1994, **132**, 87-97; (d) X. Wu, D.-G. Chen, D.

View Article Online
DOI: 10.1039/D5SC01121C

Liu, S.-H. Liu, S.-W. Shen, C.-I. Wu, G. Xie, J. Zhou, Z.-X. Huang, C.-Y. Huang, S.-J. Su, W. Zhu and P.-T. Chou, *J. Am. Chem. Soc.*, 2020, **142**, 7469-7479; (e) H. Zhang, W. Wang, C. Liu, Z. Peng, C. Du and B. Zhang, *J. Mater. Chem. C*, 2021, **9**, 9627-9636; (f) M. A. Soto, V. Carta, R. J. Andrews, M. T. Chaudhry and M. J. MacLachlan, *Angew. Chem. Int. Ed.*, 2020, **59**, 10348-10352; *Angew. Chem*. 2020, **132**, 10434-10438 (g) Y. Wang, N. Li, L. Chu, Z. Hao, J. Chen, J. Huang, J. Yan, H. Bian, P. Duan, J. Liu and Y. Fang, *Angew. Chem. Int. Ed.*, 2024, **63**, e202403898; *Angew. Chem.* 2024, **136**, e202403898; (h) H. Leopold, M. Tenne, A. Tronnier, S. Metz, I. Münster, G. Wagenblast and T. Strassner, *Angew. Chem. Int. Ed.*, 2016, **55**, 15779-15782; *Angew. Chem*. 2016, **128**, 16011 –16014.

13. K. M.-C. Wong and V. W.-W. Yam, *Coord. Chem. Rev.*, 2007, **251**, 2477-2488.
14. H. Xiang, J. Cheng, X. Ma, X. Zhou and J. J. Chruma, *Chem. Soc. Rev.*, 2013, **42**, 6128-6185.
15. (a) B. Li, Y. Li, M. H.-Y. Chan and V. W.-W. Yam, *J. Am. Chem. Soc.*, 2021, **143**, 21676-21684; (b) J. Gong and X. Zhang, *Coord. Chem. Rev.*, 2022, **453**, 214329; (c) G. Park, D. Y. Jeong, S. Y. Yu, J. J. Park, J. H. Kim, H. Yang and Y. You, *Angew. Chem. Int. Ed.*, 2023, **62**, e202309762; *Angew. Chem*. 2023, **135**, e202309762.
16. L. Chassot and A. Von Zelewsky, *Helv. Chim. Acta*, 1983, **66**, 2443-2444.
17. J. R. Brandt, X. Wang, Y. Yang, A. J. Campbell and M. J. Fuchter, *J. Am. Chem. Soc.*, 2016, **138**, 9743-9746.
18. (a) T. R. Schulte, J. J. Holstein, L. Krause, R. Michel, D. Stalke, E. Sakuda, K. Umakoshi, G. Longhi, S. Abbate and G. H. Clever, *J. Am. Chem. Soc.*, 2017, **139**, 6863-6866; (b) G. Hirata, Y. Kobayashi, R. Sato, Y. Shigeta, N. Yasuda and H. Maeda, *Chem. Eur. J.*, 2019, **25**, 8797-8804; (c) J. Song, H. Xiao, L. Fang, L. Qu, X. Zhou, Z.-X. Xu, C. Yang and H. Xiang, *J. Am. Chem. Soc.*, 2022, **144**, 2233-2244; (d) J. Song, H. Xiao, B. Zhang, L. Qu, X. Zhou, P. Hu, Z.-X. Xu and H. Xiang, *Angew. Chem. Int. Ed.*, 2023, **62**, e202302011; *Angew. Chem*. 2023, **135**, e202302011.
19. S.-Y. Yang, Y. Chen, R. T. K. Kwok, J. W. Y. Lam and B. Z. Tang, *Chem. Soc. Rev.*, 2024, **53**, 5366-5393.
20. Y. Tu, Z. Zhao, J. W. Y. Lam and B. Z. Tang, *Natl. Sci. Rev.*, 2021, **8**, nwaa260.
21. (a) J. L.-L. Tsai, T. Zou, J. Liu, T. Chen, A. O.-Y. Chan, C. Yang, C.-N. Lok and C.-M. Che, *Chem. Sci*, 2015, **6**, 3823-3830; (b) C. Y.-S. Chung and V. W.-W. Yam, *Chem. Sci*, 2013, **4**, 377-387.
22. J. S. J. Tan and R. S. Paton, *Chem. Sci*, 2019, **10**, 2285-2289.
23. D. B. Guthrie and D. P. Curran, *Org. Lett.*, 2009, **11**, 249-251.
24. E. M. Sánchez-Carnerero, A. R. Agarrabeitia, F. Moreno, B. L. Maroto, G. Muller, M. J. Ortiz and S. de la Moya, *Chem. Eur. J.*, 2015, **21**, 13488-13500.
25. X. Zhu, Z. Wang, Y. Jia, F. Yang, Y. Zhang, S. Zhao and X. He, *J. Mater. Chem. C*, 2023, **11**, 11671-11680.

The data supporting this article have been included as part of the ESI.† Deposition number 2378928, 2378929, 2378930, 2378935, 2378936, 2378939, and 2386027 contains the supplementary crystallographic data for this paper. The data can be obtained free of charge via the joint Cambridge Crystallographic Data Centre (CCDC).